Article

Halogen Bonding in Perfluoroalkyl Adsorption

Lei Lu and Chongzheng Na*

Cite This: ACS Omega 2024, 9, 26050−26057

Read Online

ACCESS | Metrics & More | Article Recommendations | SI Supporting Information

ABSTRACT: Adsorption is a promising technology to remove perfluoroalkyl substances (PFAS), including perfluorooctanesulfonic acid (PFOS) and perfluorooctanoic acid (PFOA), from contaminated water. Although a large number of materials have been evaluated for PFAS adsorption, guidelines that can facilitate the rational design and selection of adsorbents have not been established due to the lack of a mechanistic understanding on the molecular level. Using a novel interpretation of the Freundlich isotherm, this study identifies halogen bonding as the main mechanism controlling perfluoroalkyl adsorption by using a materiomic approach that compares the electrostatic polarities of a variety of carbon, polymer, and mineral-based materials reported in the literature. Comparisons show that both PFOS and PFOA are favorably adsorbed by materials containing high densities of π electrons, lone electron pairs, and negative charges, consistent with the formation of halogen bonding between the positive σ-hole of fluorine as a Lewis acid and a nucleophilic solid as a Lewis base. The identification of this previously unappreciated noncovalent bonding mechanism offers fresh insight into the search of suitable materials for perfluoroalkyl adsorption.
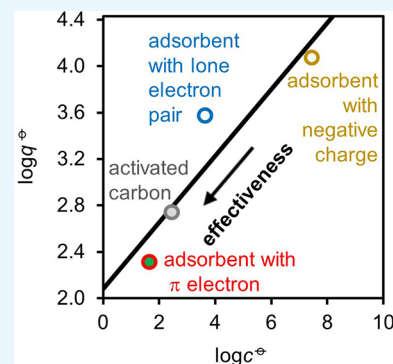
1. INTRODUCTION

Perfluoroalkyl substances (PFAS) commonly refer to amphiphilic alkyl acids with all the alkyl hydrogen (H) atoms replaced by fluorine (F).[1] The increasing detection of PFAS compounds in the environment[2,3] and concerns about their adverse effects on health, including cancer risk,[4] liver damage,[5] and immune suppression,[6] have raised the level of urgency to identify suitable technologies for PFAS removal from contaminated water.[7] Adsorption, one of the most widely used technologies in water treatment,[8,9] has been extensively evaluated for PFAS removal using both conventional and novel materials as adsorbents. Most of the studies reported in the literature agree that PFAS can be adsorbed, as well as many other organic contaminants. The studies, however, disagree on which type of material should be used to maximize the removal efficiency, particularly at low PFAS concentrations required to meet the preliminary remediation goal of 70 ppt $(ng\ L^{-1})$ that has been recently proposed by the United States Environmental Protection Agency (USEPA) for perfluorooctanesulfonic acid (PFOS; $C_7F_{17}SO_2OH$) and perfluorooctanoic acid (PFOA; $C_7F_{15}COOH$).[10]

A mechanistic understanding of PFAS-adsorbent interaction is critical to making rational design and selection of materials for PFAS adsorption.[11] Because of the high electronegativity of fluorine and the deprotonation of acids in water,[12−14] previous research has only considered the PFAS as a nucleophilic Lewis base that can be electrostatically attracted by Lewis acids such as quaternary amines attached to the adsorbent surface.[9,15] However, halogens (X) bonded to carbon in organic compounds, although being electronegative,[16] are known to be electrophilic and favor interactions with nucleophiles containing π electrons, lone electron pairs, and negative charges.[17,18] The intermolecular donor−acceptor charge transfer[19−21] between halogens and nucleophiles forms halogen bonding, similar to hydrogen bonding.[22] As shown in Figure 1, the formation of halogen bonding has been rationalized using the concept of σ-hole, which is the outermost region along the C−X bond that has positive electrostatic potentials.[23] The halogen bonding of perfluoroalkanes with amines in solution has been experimentally identified.[24] *Ab initio* calculations further suggest that the formation of halogen bonding can be promoted by the presence of electron-withdrawing groups such as sulfonic and carboxylic acids in PFAS.[15,25] Nevertheless, the importance of halogen bonding in perfluoroalkyl adsorption has not been systematically investigated.

The objective of this study is to evaluate the importance of halogen bonding in perfluoroalkyl adsorption. The evaluation is conducted by taking a materiomic approach,[26] frequently used in bioengineering[27] and crystal design[28] to establish structure−activity relationships through the meta-data analysis. To understand the preference of material electrostatic polarity in PFAS adsorption, isotherms reported in the literature are analyzed for the adsorption of PFOS and PFOA according to the Freundlich isotherm[29]:
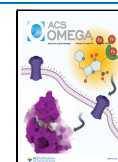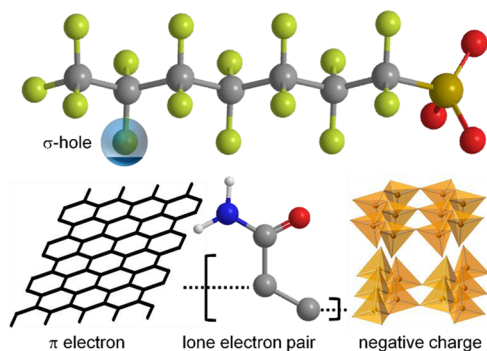
Figure 1. Schematic illustration of σ-holes in PFOS (fluorine, emerald; carbon, gray; oxygen, red) that can form halogen bonding with π electrons in graphitic carbon, lone electron pairs in polyacrylamide (nitrogen, blue; hydrogen, white; one hydrogen behind the carbon on the right), and negative charges in aluminosilicates (aluminum or silicon in the center of tetrahedron and oxygen at the apexes). See ref 25 for the potential of σ-hole plotted on the van der Waals surface.

$$q = K_F c^{1/n} \tag{1}$$

where q is the adsorption capacity, c is the perfluoroalkyl concentration in water, $1/n$ is the unitless power, and K_F is the equilibrium constant (often in $mg^{1-1/n}\ L^{1/n}\ g^{-1}$). The Gibbsian interpretation of n and K_F, which are otherwise considered to be empirical,[30−32] is used as the theoretical foundation to facilitate comparisons among carbon-, polymer-, and mineral-based adsorbents. The preference of PFOS and PFOA to be adsorbed by nucleophilic adsorbents is taken as an indication of the formation of halogen bonding.

2. METHOD

The Freundlich model is interpreted by considering the capillary effect of surface tension on adsorption.[33] According to the Gibbs equation for adsorption[34]:

$$\Gamma = -\frac{\partial \gamma}{\partial \mu} \tag{2}$$

where Γ is the surface density of PFAS, γ is the surface tension, and μ is the chemical potential of PFAS. The reduction of surface tension by PFAS adsorption can be formulated as:[35−37]

$$\partial \gamma = -\Delta h \partial \Gamma \tag{3}$$

where Δh is the change of enthalpy due to the replacement of water molecules by PFAS at the adsorbent−water interface. Combining eqs 2 and 3 with integration gives

$$\mu = \mu^{\ominus} + \Delta h \ln \frac{\Gamma}{\Gamma^{\ominus}} \tag{4}$$

where the Plimsoll symbol in the superscript denotes a hypothetical reference state of pure PFAS, R is the universal gas constant, and T is the absolute temperature. According to Gibbs,[29,30] PFAS has the same chemical potential at the interface and in water (w):

$$\mu_w = \mu_w^{\ominus} + RT \ln \frac{c_w}{c_w^{\ominus}} \tag{5}$$

Provided that M is the molecular weight of PFAS, A is the specific surface area of adsorbent, and thus:

$$q = M\Gamma A \tag{6}$$

combining eqs 4 and 5 gives

$$\log \frac{q}{q^{\ominus}} = \frac{RT}{\Delta h} \log \frac{c}{c^{\ominus}} \tag{7}$$

Comparison of eq 7 to 1 reveals that

$$n = \frac{\Delta h}{RT} \tag{8}$$

$$\log K_F = \log q^{\ominus} - \frac{1}{n} \log c^{\ominus} \tag{9}$$

where log is the 10-based logarithm. A linear correlation is, therefore, expected between $\log K_F$ and $1/n$.[38−40]
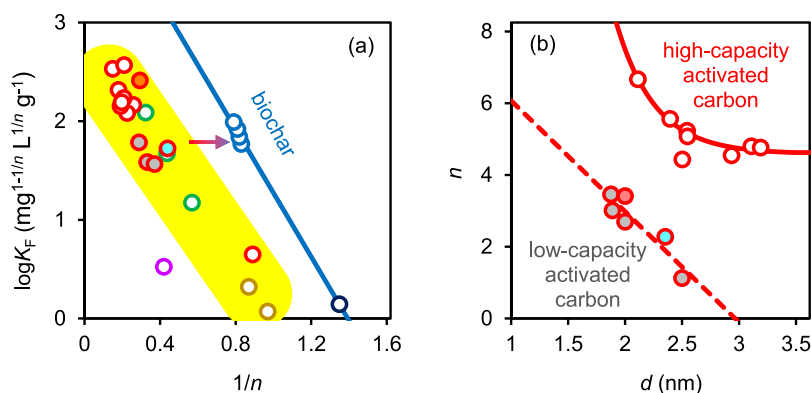

Figure 2. Adsorption of PFOS by activated carbon (red circles), carbon nanotube (green circles), black carbon (gold circles), fluorographene (purple circle), biochar (blue circles), and ash (dark blue) compared in terms of (a) the logarithm of equilibrium constant ($\log K_F$) and the power parameter ($1/n$) and (b) the inverse of power (n) and the average pore diameter (d) for activated carbon. Colors in red circles for activated carbon: white, commercial; pink, lab-made; cyan, attached to magnetite nanoparticles; gray, with high metal content. Colors in gold circles for black carbon: white, char; brown, ash. Lines in a are least-squares fits of activated carbon (red) and biochar (blue) data to eq 9, respectively. The yellow band in a is a fit to all data, except those for biochar. In b, the line is a linear fit to eq 8 for low-capacity activated carbon, and the curve is a power fit for high-capacity activated carbon. The coefficients of determination are $R^2 > 0.96$ in a and $R^2 > 0.85$ in b.

3. RESULTS AND DISCUSSION

Figure 2 compares the adsorption of PFOS by carbon-based materials reported in the literature, including activated carbon (AC, red circles),[41−49] carbon nanotube (CNT, green circles),[50] fluorographene (cyan circle),[51] black carbon (BC, gold circles),[52] and biochar (blue circles).[53] These materials differ in the extent of graphitization, as reflected by the two groups in the Freundlich plots of log K_F and $1/n$ (Figure 2a). The first group includes AC, CNT, fluorographene, and black carbon with similar degrees of graphitization, thereby aggregating in the same region (yellow band). Combining eqs 7 and 8 gives:

$$\log \frac{q}{q^{\ominus}} = \frac{1}{n}\log \frac{c}{c^{\ominus}} \tag{10}$$

The aggregation of materials in the first group indicates that they have similar values of $q^{\ominus}$ and $c^{\ominus}$; therefore, their adsorption capacities are solely determined by $1/n$ at any given value of c. Since $c < c^{\ominus}$, q increases with the decrease of $1/n$. According to eq 8, materials with low values of $1/n$ have high values of Δh, suggesting that the best materials to be used in the PFOS adsorption should induce substantial changes in interfacial enthalpy.

In comparison, biochar[53] prepared by the pyrolysis of corn straw in nitrogen gas at 250, 400, 550, and 700 °C, together with ash,[50] has a Freundlich linearity shifted to greater values of $1/n$, giving a value of $q^{\ominus}$ greater than that obtained for the first-group adsorbents. However, the exponential term $1/n$ in the equation has a dominant impact on q when the equilibrium concentration is several orders of magnitude smaller than $c^{\ominus}$. Hence, the right shift in the plot indicates that biochar and ash,[50] with reduced graphitization, are less preferred for PFOS adsorption than activated carbon and other graphitic materials. The significant reduction in the adsorption capacity of ash also corresponds to its significantly smaller carbon elemental composition (11.2 vs >60%).

The preference of PFOS adsorption with highly graphitized carbon materials is further supported by two other observations in Figure 2a. First, for the corn straw-based biochar, $1/n$ decreases and thus q increases with the increase of pyrolysis temperature,[53] consistent with the adsorption of organic compounds observed with other types of biochar materials.[54−58] Analyses of biochar structures have shown that the increase of pyrolysis temperature improves graphitization by transforming amorphous carbon to aromatic clusters and then turbostratic crystallites (i.e., small graphitic crystals misaligned at their basal planes).[59,60] Second, one AC material is made by the pyrolysis of bamboo in nitrogen gas at 500 °C (pink-filled red circle)[45] that thus should have shown similar behaviors in PFOS adsorption as the corn straw-based biochar made at a similar temperature (e.g., 550 °C) if it were used directly after pyrolysis. The material, however, becomes highly graphitized after being chemically activated in the presence of potassium hydroxide at 900 °C,[45] which is known to improve graphitization along with porosity in biochar.[61]

The positive correlation of PFOS adsorption and material graphitization supports the hypothesis that halogen bonding controls perfluoroalkyl adsorption. Graphitic carbon atoms bond with one another through three σ bonds established in three sp²-hybridized orbitals, forming a graphene sheet.[62] The remaining p_z orbital from each carbon atom is oriented perpendicular to the graphene sheet and overlaps with the p_z orbitals of other carbon atoms bonded in the sheet into a conjugated π system. The π electrons are strong nucleophiles that can form halogen bonds with the electrophilic σ-hole of fluorine in PFOS. The strength of halogen bonding is expected to be proportional to the number of electrons involved in the π system, which increases with the elimination of sp³ C associated with surface functionalization through graphitization. The importance of eliminating sp³ C to maximize PFOS adsorption is supported by the increase of $1/n$ and thus the deterioration of adsorption performance for fluorographene (purple circle).[51] In fluorographene, fluorine is bonded to carbon in graphene,[63] transforming sp² C back to sp³ C and thus reducing the nucleophilicity required for PFOS adsorption.

Compared to activated carbon, only a limited number of experimental isotherms have been reported for carbon nanotube[50] and black carbon[52] materials. CNTs are highly graphitized because they are formed by the crystal growth over metal catalysts through the chemical vapor deposition of carbon atoms.[64] The degree of graphitization can be reduced in CNTs by the formation of defects, whose density in general increases with the increase of CNT diameter.[65] This is consistent with the decrease of $1/n$ and thus the increase of PFOS adsorption with the decrease of CNT diameter (green circles in Figure 2a, diameter from left to right: 1−2, 10−20, and >50 nm).[50]

Different from CNT, black carbon (a.k.a., carbon black) is the residue of incomplete combustion.[66] As aggregates of particles consisting of graphene layers, black carbon gains a high degree of graphitization from the elimination of hydrogen and oxygen originally present in the biomass precursor through combustion.[67] The nucleophilicity of black carbon can be reduced by the presence of metal cations, which draw away π electrons in graphene from halogen bonding.

A corollary of the theory that halogen bonding controls perfluoroalkyl adsorption by carbon-based materials is that activated carbon with smaller pores should adsorb PFOS better because more fluorine atoms from the same PFAS anion can be involved in bonding with π electrons in smaller pores if PFAS can fit into the pores. Figure 2b compares n and the average pore diameter of activated carbon, d, computed from the total pore volume and the specific surface area by assuming that the pores are cylinders with a uniform diameter. The AC materials are separated into two groups and within each group, n increases and thus $1/n$ decreases with the decrease of d, as expected. The low-capacity group consists of 4 commercial AC materials (gray-filled circles),[41,42] a lab-made activated carbon (pink-filled circle),[45] and a composite of AC and magnetite (cyan-filled circle)[44] while the high-capacity group consists of 9 commercial AC materials.[46−49] The presence of the AC-magnetite composite in the low-capacity group suggests that the poor performance of the group may be caused by the detrimental effect of metal cations on halogen bonding. The high metal content in AC materials can be inherited from the precursor material[68] or result from the addition of potassium hydroxide for chemical activation.[45] In comparison, a commercial AC material known to be activated using steam and thus without the addition of a metal activator is found in the high-capacity group (white-filled circle on the far right).[46] In the high-capacity group, the increase of pore diameter induces a sharp decrease of n at $d < 2.5$ nm, which then levels off at $d > 3$ nm. This is consistent with the transition from the
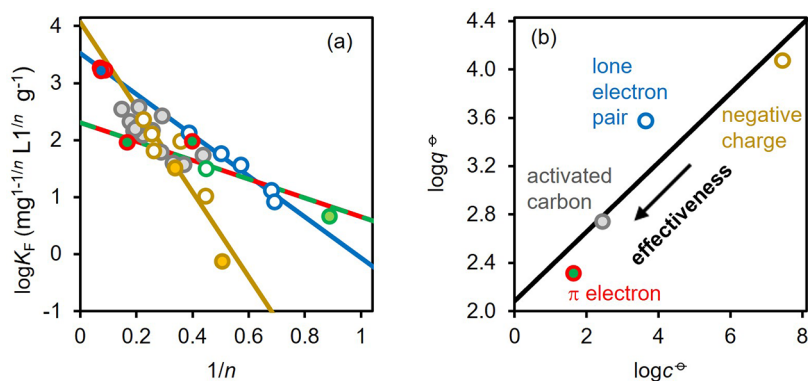
Figure 3. Adsorption of PFOS by anion-exchange resins (red circles), MOF (green circles), aluminosilicates (gold circles), and polymers other than anion-exchange resins (blue circles), together with activated carbon shown in Figure 2a (gray), compared in terms of (a) the logarithm of equilibrium constant (log K_F) and the power parameter ($1/n$) and (b) the logarithms of adsorption capacity and PFOS concentration at the reference state (log $q^{\ominus}$ and log $c^{\ominus}$) obtained from fitting log K_F and $1/n$ to eq 9. Colors used are as follows: green, macroreticular polystyrene divinylbenzene; blue, polyacrylamide gel. Colors in gold circles: white, montmorillonite; orange, zeolite. Colors in green circles: white, UiO-66 MOF; emerald, SCU-8 MOF. Lines in a are least-squares fits to eq 9: green-red, all green circles and green-filled red circles for the group of materials having π electrons; blue, all blue circles and the blue-filled red circle for the group having lone electron pairs; gold, all gold circles for the group with negative charges, with coefficients of determination of R^2 = 0.94, 0.96, and 0.84. The line in b is a linear fit of all data to eq 11 with R^2 = 0.87.

positioning of PFOS in the middle of a pore to its attachment on one side of the pore as d increases.

Figure 3a compares PFOS adsorption by polymer and mineral-based materials, including anion-exchange resins (red circles),[43,46,69−71] metal−organic frameworks (MOF; green circles),[46,72,73] aluminosilicates (gold circles),[41,49,74] and polymers other than anion-exchange resins (blue circles).[75] These materials can be regrouped according to their molecular structures associated with nucleophilic electrons. First, macroreticular[76] resins containing divinylbenzene[77] (green-filled red circles) are grouped with MOFs because they both have aromatic rings with π electrons. Second, the resin based on the polyacrylic matrix (blue-filled red circle) is grouped with polyacrylamide[78] and polysaccharide polymers that contain oxygen and nitrogen with lone electron pairs. Last, mineral-based materials such as montmorillonite and zeolite are categorized as one group since their aluminosilicate frameworks, which gain negative charges from the isomorphic substitution of silicon (Si^{4+}) by aluminum (Al^{3+}) in the oxygen tetrahedron.[79] Because the balancing cations are either intercalated between aluminosilicate sheets[80] or confined in aluminosilicate micropores[81] with complete separation, these frameworks can form nucleophilic interactions with PFOS adsorbed between sheets or inside pores.

The ranking of material preference in PFOS adsorption is correlated with the material electron density, as supported by several observations in Figure 3a within a material group. In the π-electron group (green and green-filled red circles), the anion-exchange resin,[43] with styrene and divinylbenzene as the framework, shows the best PFOS adsorption. UiO-66 MOF (white-filled green circles)[46] shows better PFOS adsorption than SCU-8 MOF (emerald-filled green circles),[72] which can be explained by the pore size effect of electron density (0.6 nm vs 2.2 nm).[46,72] When UiO-66 is synthesized with perfluoroterephthalic acid ($C_6F_4(COOH)_2$) in place of terephthalic acid ($C_6H_4(COOH)_2$; white-filled green circles),[73] log K_F and $1/n$ are estimated to be 0.37 (K_F in mg$^{-0.2}$ L$^{1.2}$ g^{-1}) and 1.2, representing a poor performance of PFOS adsorption that falls off the scales of Figure 3a. The sharp reduction in performance

is caused by the formation of a positive π-hole around the aromatic ring by fluorination,[82] which converts the nucleophilic terephthalic acid to the electrophilic perfluoroterephthalic acid.

In the group having lone electron pairs, similar to the π-electron group, the anion-exchange resins made of polyacrylic framework (blue-filled red circle)[70,71] also significantly outperform both poly glycidyl methacrylate (first white-filled blue circle on the left)[69] and chitosan (remaining white-filled blue circles).[75]

In the aluminosilicate group, intercalating hexadecyltrimethylammonium in montmorillonite (white-filled gold circles except one on the very right for montmorillonite), which increases the electron density between aluminosilicate sheets as the singly charged surfactant cation pushes out many sodium cations, is shown to enhance PFOS adsorption.[83] The high charge density also allows modified montmorillonites to outperform zeolites (orange-filled gold circles). The NaY zeolite with a pore diameter of 0.6 nm performs better than the 13X zeolite with a pore diameter of 1.3 nm, likely due to the pore size effect of electron density that has been discussed for activated carbon (cf. Figure 2b).

Figure 3b compares log $q^{\ominus}$ and log $c^{\ominus}$ obtained from least-squares fits of log K_F and $1/n$ to eq 9 for all three material groups, together with log $q^{\ominus}$ and log $c^{\ominus}$ for activated carbon. The linear correlation of the four sets of log $q^{\ominus}$ and log $c^{\ominus}$ supports that the wide range of materials tested for PFOS adsorption share the same mechanism of electrostatic attraction through halogen bonding. Provided that $1/n_0$ and log $q_0^{\ominus}$ are used to represent the slope and intercept of the linearity:

$$\log q^{\ominus} = \frac{1}{n_0}\log c^{\ominus} + \log q_0^{\ominus} \tag{11}$$
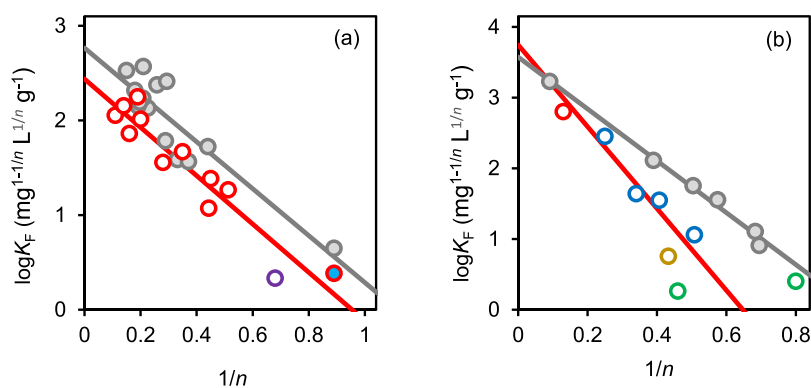
Combining eq 11 with eq 10 gives

Figure 4. Adsorption of PFOA (colored circles) by (a) carbon-based and (b) polymer/mineral-based materials, together with the adsorption of PFOS (gray circles) adsorption by (a) activated carbon and (b) polymers containing lone electron pairs, compared in terms of the logarithm of equilibrium constant (log K_F) and the power parameter ($1/n$). Symbols other than gray circles in *a*: white-filled red circles, commercial activated carbon; purple circle, activated carbon attached on magnetite nanoparticles; cyan-filled red circle, fluorographene. Symbols other than gray circles in *b*: red circle, resin; blue circles, oxygen/nitrogen-containing polymers; green circles, metal−organic framework. Red lines are linear fits of PFOA adsorption to eq 9 with coefficients of determination of $R^2 > 0.78$.

$$\log q = \frac{1}{n}\log c - \left(1 - \frac{1}{n_0}\right)\log c^{\ominus} + \log q_0^{\ominus} \quad (12)$$

Regression Figure 3b gives $1/n_0 = 0.28 > 0$; therefore, q and thus the effectiveness of halogen bonding increases with the decrease of $c^{\ominus}$ according to eq 12. However, when $1/n$ is very small with an extremely high electron density, q is predominately controlled by the first term of eq 12 with a negligible contribution from the second term, suggesting that the type of material used in PFOS adsorption no longer affects the adsorption capacity.

Figure 4 shows the adsorption of PFOA (red circles) by (a) carbon-based and (b) polymer/mineral-based materials in comparison to the adsorption of PFOS (gray circles) by (a) activated carbon and (b) polymers containing lone electron pairs. In comparison to the large number of materials tested for PFOS adsorption, only a limited number of materials have been studied for PFOA adsorption with the same rigor. As shown in Figure 4a, most of the carbon-based materials used for PFOA adsorption are commercial activated carbon samples (white-filled red circles)[41−43,45,47,72,84] except for two samples being AC attached to magnetite nanoparticles (purple circle)[44] and fluorographene (cyan-filled red circle).[51] Regression of log K_F and $1/n$ for these samples to eq 9 shows good linearity (red line), with estimates of close $c^{\ominus}$ and smaller $q^{\ominus}$ than those for PFOS adsorption by activated carbon (gray line). According to eq 10, q is predominantly determined by $c^{\ominus}$ when $1/n \ll 1$, indicating that carbon-based materials prefer the adsorption PFOS over PFOA. A similar conclusion can be made for polymer/mineral materials,[43,49,69,73,74,85−87] as shown in Figure 4b. The preference of PFOS over PFOA in adsorption is consistent with the ability of PFOS to form stronger halogen bonding than PFOA. Since sulfonate is more electron-withdrawing than carboxylate, fluorine is expected to have a greater σ-hole in PFOS to promote adsorption.[88,89]

In summary, the formation of halogen bonding as the molecular mechanism controlling perfluoroalkyl adsorption is supported by the preference for PFOS and PFOA to be adsorbed by electrophilic Lewis-base solids containing high densities of π electrons, lone electron pairs, and negative charges. In addition to water treatment, understanding the importance of halogen bonding in the adsorption of perfluorinated compounds may also help elucidate the reductive defluorination of PFAS by microorganisms,[90] given the high density of π electrons and lone electron pairs in enzymes.[91] As for PFAS adsorption, the best material reported in the literature is polyacrylic resins, which has $1/n = 0.072$ and log $K_F = 3.26$ for PFOS adsorption[71] (blue-filled red circle in Figure 3a) and $1/n = 0.13$ and log $K_F = 2.80$ for PFOA adsorption (red circle in Figure 4b).[43] According to eq 9, the adsorption capacity becomes insensitive to the change of solution concentration, with these extremely low values of $1/n$. At 70 ng L^{-1}, the remediation goal proposed by USEPA,[10] each gram of the resin can adsorb up to 913 mg of PFOS and 183 mg of PFOA. In comparison to the polyacrylamide resin, the best-activated carbon has $1/n = 0.15$ and log $K_F = 2.53$ for PFOS adsorption (the very left white-filled red circle in Figure 2a) and $1/n = 0.11$ and log $K_F = 2.05$ for PFOA adsorption (red circle in Figure 4b),[47] giving an adsorption capacity of $q = 80$ and 39 mg g^{-1}, respectively. Whether these ultrahigh capacities can materialize in practice awaits experimental evaluation.

PFASs are a large family of compounds. According to the Organization for Economic Co-operation and Development (OECD), the PFAS family includes all compounds containing at least one saturated CF_2 or CF_3 moiety with more than 7 million members.[92] Among them, neutral PFAS compounds such as perfluoroalkyl iodides possess completely different molecular characteristics compared to common target acids such as PFOS and PFOA and thus may require further research to determine their adsorption mechanisms. In addition, functional groups other than fluorine can also influence PFAS adsorption through interactions, such as hydrogen bonding. The competition and cooperation of these factors with halogen bonding remain to be explored in future studies.

ASSOCIATED CONTENT

ⓈI Supporting Information

The Supporting Information is available free of charge at https://pubs.acs.org/doi/10.1021/acsomega.4c01367.

> Values of Freundlich parameters for PFOS and PFOA adsorption by different materials obtained from the literature (PDF)

■ AUTHOR INFORMATION

Corresponding Author

Chongzheng Na − *Department of Civil, Environmental and Construction Engineering, Texas Tech University, Lubbock, Texas 79409, United States;* ⊙ orcid.org/0000-0002-5849-6817; Phone: 1-806-834-3597; Email: chongzheng.na@outlook.com

Author

Lei Lu − *Department of Civil, Environmental and Construction Engineering, Texas Tech University, Lubbock, Texas 79409, United States;* ⊙ orcid.org/0009-0005-5607-5938

Complete contact information is available at:
https://pubs.acs.org/10.1021/acsomega.4c01367

Notes

The authors declare no competing financial interest.

■ REFERENCES

(1) Prevedouros, K.; et al. Sources, fate and transport of perfluorocarboxylates. *Environ. Sci. Technol.* **2006**, *40* (1), 32−44.

(2) Harrad, S.; et al. Perfluoroalkyl substances in drinking water, indoor air and dust from Ireland: Implications for human Exposure. *Environ. Sci. Technol.* **2019**, *53* (22), 13449−13457.

(3) Guelfo, J. L.; Adamson, D. T. Evaluation of a national data set for insights into sources, composition, and concentrations of per- and polyfluoroalkyl substances (PFASs) in U.S. drinking water. *Environ. Pollut.* **2018**, *236*, 505−513.

(4) Steenland, K.; Winquist, A. PFAS and cancer, a scoping review of the epidemiologic evidence. *Environmental research* **2021**, *194*, No. 110690.

(5) Ducatman, A.; Fenton, S. E. Invited perspective: PFAS and liver disease: bringing all the evidence together. *Environ. Health Perspect.* **2022**, *130* (4), No. 041303.

(6) Rudzanova, B.; et al. Impact of PFAS exposure on prevalence of immune-mediated diseases in adults in the Czech Republic. *Environmental Research* **2023**, *229*, No. 115969.

(7) Andersen, M. E.; et al. Perfluoroalkyl acids and related chemistries—Toxicokinetics and modes of action. *Toxicol. Sci.* **2008**, *102* (1), 3−14.

(8) Rahman, M. F.; Peldszus, S.; Anderson, W. B. Behaviour and fate of perfluoroalkyl and polyfluoroalkyl substances (PFASs) in drinking water treatment: A review. *Water Res.* **2014**, *50*, 318−340.

(9) Du, Z. W.; et al. Adsorption behavior and mechanism of perfluorinated compounds on various adsorbents-A review. *Journal of Hazardous Materials* **2014**, *274*, 443−454.

(10) United States Environmental Protection Agency. *EPA's Per- and Polyfluoroalkyl Substances (PFAS) Action Plan*; EPA, **2020**.

(11) Polanyi, M. The potential theory of adsorption. *Science* **1963**, *141* (3585), 1010−1013.

(12) Goss, K.-U. The pKa values of PFOA and other highly fluorinated carboxylic acids. *Environ. Sci. Technol.* **2008**, *42* (2), 456−458.

(13) Brooke, D.; Footitt, A.; Nwaogu, T. A. *Environmental Risk Evaluation Report: Perfluorooctanesulphonate (PFOS)*; United Kingdom Environment Agency, 2004.

(14) Burns, D. C.; et al. Experimental pKa determination for perfluorooctanoic acid (PFOA) and the potential impact of pKa concentration dependence on laboratory-measured partitioning phenomena and environmental modeling. *Environ. Sci. Technol.* **2008**, *42* (24), 9283−9288.

(15) Ateia, M.; et al. Efficient PFAS removal by amine-functionalized sorbents: critical review of the current literature. *Environmental Science & Technology Letters* **2019**, *6* (12), 688−695.

(16) Pauling, L. The nature of the chemical bond. IV. The energy of single bonds and the relative electronegativity of atoms. *J. Am. Chem. Soc.* **1932**, *54* (9), 3570−3582.

(17) Duarte, D. J. R.; De las Vallejos, M. M.; Peruchena, N. M. Topological analysis of aromatic halogen/hydrogen bonds by electron charge density and electrostatic potentials. *J. Mol. Model.* **2010**, *16* (4), 737−748.

(18) Cavallo, G.; et al. The halogen bond. *Chem. Rev.* **2016**, *116* (4), 2478−2601.

(19) Mulliken, R. S. Structures of complexes formed by halogen molecules with aromatic and with oxygenated solvents. *J. Am. Chem. Soc.* **1950**, *72* (1), 600−608.

(20) Hassel, O. Structural aspects of interatomic charge-transfer bonding. *Science* **1970**, *170* (3957), 497−502.

(21) Desiraju, G. R.; et al. Definition of the halogen bond (IUPAC Recommendations 2013). *Pure Appl. Chem.* **2013**, *85* (8), 1711−1713.

(22) Metrangolo, P.; et al. Halogen bonding based recognition processes: A world parallel to hydrogen bonding. *Acc. Chem. Res.* **2005**, *38* (5), 386−395.

(23) Clark, T.; et al. Halogen bonding: The σ-hole. *J. Mol. Model.* **2007**, *13* (2), 291−296.

(24) Burdeniuc, J.; Sanford, M.; Crabtree, R. H. Amine charge transfer complexes of perfluoroalkanes and an application to poly(tetrafluoroethylene) surface functionalization. *J. Fluorine Chem.* **1998**, *91* (1), 49−54.

(25) Metrangolo, P.; et al. Fluorine-centered halogen bonding: a factor in recognition phenomena and reactivity. *Cryst. Growth Des.* **2011**, *11* (9), 4238−4246.

(26) Cranford, S.; Buehler, M. J. Materiomics: Biological protein materials, from nano to macro. *Nanotechnol. Sci. Appl.* **2010**, *3*, 127−148.

(27) Saraogi, I.; et al. C-halogen···π interactions in proteins: A database study. *Crystal Engineering* **2003**, *6* (2), 69−77.

(28) Taylor, R.; Wood, P. A. A million crystal structures: The whole is greater than the sum of its parts. *Chem. Rev.* **2019**, *119* (16), 9427−9477.

(29) Freundlich, H. Über die Adsorption in Lösungen. *Zeitschrift für Physikalische Chemie* **1907**, *57U* (1), 385−470.

(30) Skopp, J. Derivation of the Freundlich adsorption isotherm from kinetics. *Journal of chemical education* **2009**, *86* (11), 1341.

(31) Halsey, G. Physical adsorption on non-uniform surfaces. *J. Chem. Phys.* **1948**, *16* (10), 931−937.

(32) Sips, R. On the structure of a catalyst surface. *J. Chem. Phys.* **1948**, *16* (5), 490−495.

(33) Gibbs, J. W. On the equilibrium of heterogeneous substances. *Am. J. Sci.* **1878**, *16*, 441−458.

(34) Andrews, D. H. et al. *Commentary on the Scientific Papers of J. Willard Gibbs: Vol. I Thermodynamics*; Yale University Press: New Haven, 1936.

(35) Lunkenheimer, K.; Geggel, K.; Prescher, D. Role of counterion in the adsorption behavior of 1:1 ionic surfactants at fluid interfaces—Adsorption properties of alkali perfluoro-n-octanoates at the air/water interface. *Langmuir* **2017**, *33* (39), 10216−10224.

(36) Lyu, Y.; et al. Adsorption of PFOA at the air-water interface during transport in unsaturated porous media. *Environ. Sci. Technol.* **2018**, *52* (14), 7745−7753.

(37) Costanza, J.; et al. Accumulation of PFOA and PFOS at the air−water interface. *Environmental Science & Technology Letters* **2019**, *6* (8), 487−491.

(38) Abe, I.; et al. Relationship between the Freundlich adsorption constants K and 1/N hydrophobic adsorption. *J. Am. Chem. Soc.* **1982**, *104* (23), 6452−6453.

(39) Ebato, M.; Yonebayashi, K. Relationship between Freundlich isotherm coefficients, log K_F and 1/n for atrazine desorption from soils in Japan. *Soil Science and Plant Nutrition* **2003**, *49* (5), 677−683.

(40) Ebato, M.; Yonebayashi, K.; Kosaki, T. Predicting Freundlich adsorption isotherm of atrazine on Japanese soils. *Soil Science and Plant Nutrition* **2001**, *47* (2), 221−231.

(41) Ochoa-Herrera, V.; Sierra-Alvarez, R. Removal of perfluori-nated surfactants by sorption onto granular activated carbon, zeolite and sludge. *Chemosphere* **2008**, *72* (10), 1588−1593.

(42) Zhang, D.; et al. Sorption of perfluorooctanoic acid, perfluorooctane sulfonate and perfluoroheptanoic acid on granular activated carbon. *Chemosphere* **2016**, *144*, 2336−2342.

(43) Yu, Q.; et al. Sorption of perfluorooctane sulfonate and perfluorooctanoate on activated carbons and resin: Kinetic and isotherm study. *Water research* **2009**, *43* (4), 1150−1158.

(44) Meng, P. P.; et al. Efficient removal of perfluorinated compounds from water using a regenerable magnetic activated carbon. *Chemosphere* **2019**, *224*, 187−194.

(45) Deng, S.; et al. Enhanced adsorption of perfluorooctane sulfonate and perfluorooctanoate by bamboo-derived granular activated carbon. *Journal of hazardous materials* **2015**, *282*, 150−157.

(46) Clark, C. A.; et al. Highly defective UiO-66 materials for the adsorptive removal of perfluorooctanesulfonate. *ACS Sustainable Chem. Eng.* **2019**, *7* (7), 6619−6628.

(47) Chen, W.; et al. Sorption of perfluorooctane sulfonate and perfluorooctanoate on polyacrylonitrile fiber-derived activated carbon fibers: in comparison with activated carbon. *RSC Adv.* **2017**, *7* (2), 927−938.

(48) Liang, X. Q.; et al. Facile preparation of magnetic separable powdered-activated-carbon/Ni adsorbent and its application in removal of perfluorooctane sulfonate (PFOS) from aqueous solution. *Journal of Environment Science and Health, Part A Environmental Science* **2011**, *46* (13), 1482−1490.

(49) Du, Z.; et al. Selective and high sorption of perfluorooctanesul-fonate and perfluorooctanoate by fluorinated alkyl chain modified montmorillonite. *J. Phys. Chem. C* **2016**, *120* (30), 16782−16790.

(50) Chen, X.; et al. A comparative study on sorption of perfluorooctane sulfonate (PFOS) by chars, ash and carbon nanotubes. *Chemosphere* **2011**, *83* (10), 1313−1319.

(51) Wang, W. J.; et al. Rapid and efficient removal of organic micropollutants from environmental water using a magnetic nano-particles-attached fluorographene-based sorbent. *Chemical Engineering Journal* **2018**, *343*, 61−68.

(52) Chen, H.; et al. Sorption of perfluorooctane sulfonate (PFOS) on oil and oil-derived black carbon: Influence of solution pH and [Ca2+]. *Chemosphere* **2009**, *77* (10), 1406−1411.

(53) Guo, W.; et al. Adsorption of perfluorooctane sulfonate (PFOS) on corn straw-derived biochar prepared at different pyrolytic temperatures. *Journal of the Taiwan Institute of Chemical Engineers* **2017**, *78*, 265−271.

(54) Sun, K.; et al. Variation in sorption of propiconazole with biochars: The effect of temperature, mineral, molecular structure, and nano-porosity. *Chemosphere* **2016**, *142*, 56−63.

(55) Chen, B.; Zhou, D.; Zhu, L. Transitional adsorption and partition of nonpolar and polar aromatic contaminants by biochars of pine needles with different pyrolytic temperatures. *Environ. Sci. Technol.* **2008**, *42* (14), 5137−5143.

(56) Chen, B.; Chen, Z. Sorption of naphthalene and 1-naphthol by biochars of orange peels with different pyrolytic temperatures. *Chemosphere* **2009**, *76* (1), 127−133.

(57) Li, J.; et al. A comparison of biochars from lignin, cellulose and wood as the sorbent to an aromatic pollutant. *Journal of Hazardous Materials* **2014**, *280*, 450−457.

(58) Kearns, J. P.; et al. 2,4-D adsorption to biochars: Effect of preparation conditions on equilibrium adsorption capacity and comparison with commercial activated carbon literature data. *Water Res.* **2014**, *62*, 20−28.

(59) Keiluweit, M.; et al. Dynamic molecular structure of plant biomass-derived black carbon (biochar). *Environ. Sci. Technol.* **2010**, *44* (4), 1247−1253.

(60) Xiao, X.; Chen, B. A direct observation of the fine aromatic clusters and molecular structures of biochars. *Environ. Sci. Technol.* **2017**, *51* (10), 5473−5482.

(61) Wang, J.; Kaskel, S. KOH activation of carbon-based materials for energy storage. *J. Mater. Chem.* **2012**, *22* (45), 23710−23725.

(62) Freise, E. J. Structure of graphite. *Nature* **1962**, *193* (4816), 671−672.

(63) Nair, R. R.; et al. Fluorographene: A two-dimensional counterpart of Teflon. *Small* **2010**, *6* (24), 2877−2884.

(64) Raty, J.-Y.; Gygi, F.; Galli, G. Growth of carbon nanotubes on metal nanoparticles: A microscopic mechanism from ab initio molecular dynamics simulations. *Phys. Rev. Lett.* **2005**, *95* (9), No. 096103.

(65) Charlier, J. C. Defects in carbon nanotubes. *Acc. Chem. Res.* **2002**, *35* (12), 1063−1069.

(66) Glaser, B.; et al. Black carbon in soils: The use of benzenecarboxylic acids as specific markers. *Org. Geochem.* **1998**, *29* (4), 811−819.

(67) Khodabakhshi, S.; Fulvio, P. F.; Andreoli, E. Carbon black reborn: Structure and chemistry for renewable energy harnessing. *Carbon* **2020**, *162*, 604−649.

(68) Arnold, R. G. et al. *In-situ Regeneration of Granular Activated Carbon (GAC) Using Fenton's Reagents*; United States Environmental Protection Agency, **2007**.

(69) Deng, S.; et al. Adsorption of perfluorinated compounds on aminated rice husk prepared by atom transfer radical polymerization. *Chemosphere* **2013**, *91* (2), 124−130.

(70) Gao, Y.; et al. Adsorptive removal of emerging polyfluoroalky substances F-53B and PFOS by anion-exchange resin: A comparative study. *Journal of Hazardous Materials* **2017**, *323*, 550−557.

(71) Deng, S.; et al. Removal of perfluorooctane sulfonate from wastewater by anion exchange resins: Effects of resin properties and solution chemistry. *Water Res.* **2010**, *44* (18), 5188−5195.

(72) Li, Y.; et al. A mesoporous cationic thorium-organic framework that rapidly traps anionic persistent organic pollutants. *Nat. Commun.* **2017**, *8* (1), 1354.

(73) Sini, K.; et al. Metal−organic framework sorbents for the removal of perfluorinated compounds in an aqueous environment. *New J. Chem.* **2018**, *42* (22), 17889−17894.

(74) Zhou, Q.; et al. Sorption of perfluorooctane sulfonate on organo-montmorillonites. *Chemosphere* **2010**, *78* (6), 688−694.

(75) Yu, Q.; Deng, S.; Yu, G. Selective removal of perfluorooctane sulfonate from aqueous solution using chitosan-based molecularly imprinted polymer adsorbents. *Water Res.* **2008**, *42* (12), 3089−3097.

(76) Kunin, R.; Meitzner, E.; Bortnick, N. Macroreticular ion exchange resins. *J. Am. Chem. Soc.* **1962**, *84* (2), 305−306.

(77) Ezzeldin, H. A.; Apblett, A.; Foutch, G.L. Synthesis and properties of anion exchangers derived from chloromethyl styrene codivinylbenzene and their use in water treatment. *Int. J. Polymer Sci.* **2010**, *2010*, No. 684051, DOI: 10.1155/2010/684051.

(78) Thompson, K.; Michielsen, S. Novel synthesis of N-substituted polyacrylamides: Derivatization of poly(acrylic acid) with amines using a triazine-based condensing reagent. *J. Polym. Sci., Part A: Polym. Chem.* **2006**, *44* (1), 126−136.

(79) Akgül, M.; et al. Removal of silver (I) from aqueous solutions with clinoptilolite. *Microporous Mesoporous Mater.* **2006**, *94* (1), 99−104.

(80) Viani, A.; Gualtieri, A.; Artioli, G. The nature of disorder in montmorillonite by simulation of X-ray powder patterns. *Am. Mineral.* **2002**, *87*, 966 DOI: 10.2138/am-2002-0720.

(81) Smyth, J. R.; Spaid, A. T.; Bish, D. L. Crystal structures of a natural and a Cs-exchanged clinoptilolite. *Am. Mineral.* **1990**, *75* (5−6), 522−528.

(82) Wang, H.; Wang, W.; Jin, W. J. σ-hole bond vs π-hole bond: A comparison based on halogen bond. *Chem. Rev.* **2016**, *116* (9), 5072−5104.

(83) Zhou, Q.; et al. Mechanism of p-nitrophenol adsorption from aqueous solution by HDTMA$^+$-pillared montmorillonite—Implications for water purification. *Journal of Hazardous Materials* **2008**, *154* (1), 1025−1032.

(84) Qu, Y.; et al. Equilibrium and kinetics study on the adsorption of perfluorooctanoic acid from aqueous solution onto powdered activated carbon. *Journal of Hazardous Materials* **2009**, *169* (1−3), 146−152.

(85) Ateia, M.; et al. Rapid removal of poly- and perfluorinated alkyl substances by poly(ethylenimine)-functionalized cellulose microcrystals at environmentally relevant conditions. *Environmental Science & Technology Letters* **2018**, *5* (12), 764−769.

(86) Gong, Y.; et al. Removal of aqueous perfluorooctanoic acid (PFOA) using starch-stabilized magnetite nanoparticles. *Science of The Total Environment* **2016**, *562*, 191−200.

(87) Li, J.; et al. Removal of perfluorooctanoic acid from water with economical mesoporous melamine-formaldehyde resin microsphere. *Chemical Engineering Journal* **2017**, *320*, 501−509.

(88) Lim, J. Y.; Beer, P. D. Sigma-hole interactions in anion recognition. *Chem.* **2018**, *4* (4), 731−783.

(89) Politzer, P.; Murray, J. S.; Clark, T. Halogen bonding and other σ-hole interactions: A perspective. *Phys. Chem. Chem. Phys.* **2013**, *15* (27), 11178−11189.

(90) Huang, S.; Jaffé, P. R. Defluorination of perfluorooctanoic acid (PFOA) and perfluorooctane sulfonate (PFOS) by Acidimicrobium sp. Strain A6. *Environmental Science & Technology* **2019**, *53* (19), 11410−11419.

(91) Gilday, L. C.; et al. Halogen bonding in supramolecular chemistry. *Chem. Rev.* **2015**, *115* (15), 7118−7195.

(92) Schymanski, E. L.; et al. Per- and Polyfluoroalkyl Substances (PFAS) in PubChem: 7 Million and Growing. *Environ. Sci. Technol.* **2023**, *57* (44), 16918−16928.